Vertical Directionality of Midfrequency Surface Noise in Downward-Refracting Environments

Cathy Ann Clark, *Member, IEEE*

***Abstract*—The vertical directionality of ambient noise due to surface agitation for frequencies between 2 and 5 kHz propagated to a subsurface receiver has a characteristic shape, knowledge of which may enhance shallow-water operations. In general, the noise level is highest at upward-looking angles and attenuated at downward-looking angles depending on the nature of the bottom. In environments with a negative profile gradient, the noise level is also greatly reduced in a low-angle shadow zone or "notch" at angles around horizontal. This paper reviews the character of vertical noise directionality by examining two measured data sets and considering the underlying physical mechanisms that drive the form of the distribution. A discussion of the implications of vertical noise directionality for design and operation of receiving sonar systems is presented. In particular, the effect of mainlobe beamwidth and sidelobe suppression are considered along with the directionality of the noise field. Finally, an overview of the derivation of a vertical noise model based on the integrated mode method of propagation prediction is followed by model reproduction of measurements.**

***Index Terms*—Acoustics, ambient noise, surface noise, underwater sound propagation, vertical noise distribution.**

I. Introduction

In the absence of near-shipping interference, the undersea ambient field in the frequency band of 0.5–10 kHz is dominated by noise due to sea surface roughness as shown in Fig. 1[1]. Although near and distant shipping along with other undersea acoustic effects such as internal waves are also factors in the ambient noise field, this paper addresses only the impact of midfrequency noise resulting from sea surface agitation near a submerged receiver in downward-refracting environments. The data sets studied were taken in scenarios dominated by sea surface noise, and the shipping components of the noise model described in Section IV are not discussed herein.

A significant amount of research has been done in an attempt to quantify and explain the dependence of underwater noise on wind speed and surface agitation [2]–[4], yet the exact nature of the coupling of energy from surface agitation due to wind and sea state into acoustic pressure waves that propagate through the undersea environment is an area of ongoing research [5]–[7]. It is believed by several researchers that the source of surface noise is breaking waves and whitecaps which results in the projection of bubbles into the water column, e.g., [4]–[7].

It has been shown that dipole and monopole models of the source function tend to apply at high and low frequencies, respectively [8]. For the purposes of this paper, we assume that bubbles from the surface radiate as monopoles. The location of a monopole source below a pressure-release surface results in a dipole-like propagation pattern from the perspective of a subsurface receiver. Propagation of each source through the environment and superposition of pressure (or intensity) at the position of a submerged receiver yield the noise distribution as a function of vertical angle at a given azimuth. Further discussion of the source and propagation functions is given in Section IV-A.

The ambient noise field in the undersea medium as perceived through a sonar system is tactically relevant with respect to a signal arriving simultaneously at the same sonar receiver. The 3-D convolution of the noise field with a given system beam yields the beam noise level associated with a given steer angle. Repetition over a set of vertically directional beams yields the distribution of beam ambient noise as a function of beam depression/elevation (D/E) angle. For operational use, ambient

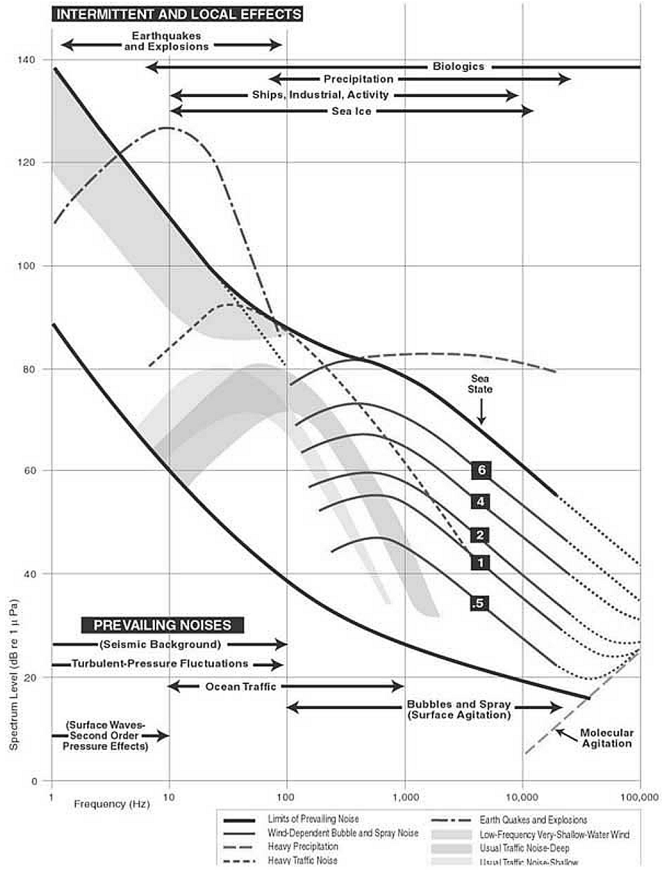

Fig. 1. Acoustic ambient noise in the ocean (adapted from [1] by the National Academy of Sciences).

Manuscript received September 28, 2005; revised March 29, 2007; accepted June 19, 2007.

Associate Editor: D. P. Knobles.

The author is with the Naval Undersea Warfare Center, Newport, RI 02841 USA (e-mail: clarkca@npt.nuwc.navy.mil).

Digital Object Identifier 10.1109/JOE.2007.903450

Report Documentation Page

Form Approved
OMB No. 0704-0188

1. REPORT DATE	2. REPORT TYPE	3. DATES COVERED
29 MAR 2007		**00-00-2007 to 00-00-2007**

4. TITLE AND SUBTITLE	5a. CONTRACT NUMBER
Vertical Directionality of Midfrequency Surface Noise in Downward-Refracting Environments	5b. GRANT NUMBER
	5c. PROGRAM ELEMENT NUMBER
6. AUTHOR(S)	5d. PROJECT NUMBER
	5e. TASK NUMBER
	5f. WORK UNIT NUMBER
7. PERFORMING ORGANIZATION NAME(S) AND ADDRESS(ES) **Naval Undersea Warfare Center,Newport Division,Newport,RI,02841**	8. PERFORMING ORGANIZATION REPORT NUMBER
9. SPONSORING/MONITORING AGENCY NAME(S) AND ADDRESS(ES)	10. SPONSOR/MONITOR'S ACRONYM(S)
	11. SPONSOR/MONITOR'S REPORT NUMBER(S)

12. DISTRIBUTION/AVAILABILITY STATEMENT
Approved for public release; distribution unlimited

13. SUPPLEMENTARY NOTES

14. ABSTRACT
The vertical directionality of ambient noise due to surface agitation for frequencies between 2 and 5 kHz propagated to a subsurface receiver has a characteristic shape, knowledge of which may enhance shallow-water operations. In general, the noise level is highest at upward-looking angles and attenuated at downward- looking angles depending on the nature of the bottom. In environments with a negative profile gradient, the noise level is also greatly reduced in a low-angle shadow zone or ?notch? at angles around horizontal. This paper reviews the character of vertical noise directionality by examining two measured data sets and considering the underlying physical mechanisms that drive the form of the distribution. A discussion of the implications of vertical noise directionality for design and operation of receiving sonar systems is presented. In particular, the effect of mainlobe beamwidth and sidelobe suppression are considered along with the directionality of the noise field. Finally, an overview of the derivation of a vertical noise model based on the integrated mode method of propagation prediction is followed by model reproduction of measurements.

15. SUBJECT TERMS

16. SECURITY CLASSIFICATION OF:			17. LIMITATION OF ABSTRACT	18. NUMBER OF PAGES	19a. NAME OF RESPONSIBLE PERSON
a. REPORT **unclassified**	b. ABSTRACT **unclassified**	c. THIS PAGE **unclassified**	**Same as Report (SAR)**	**11**	

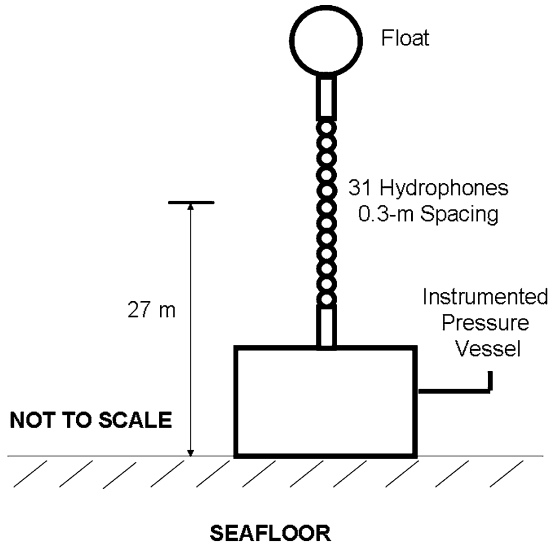

Fig. 2. NDABS used to collect GOM data (reproduced from [10]).

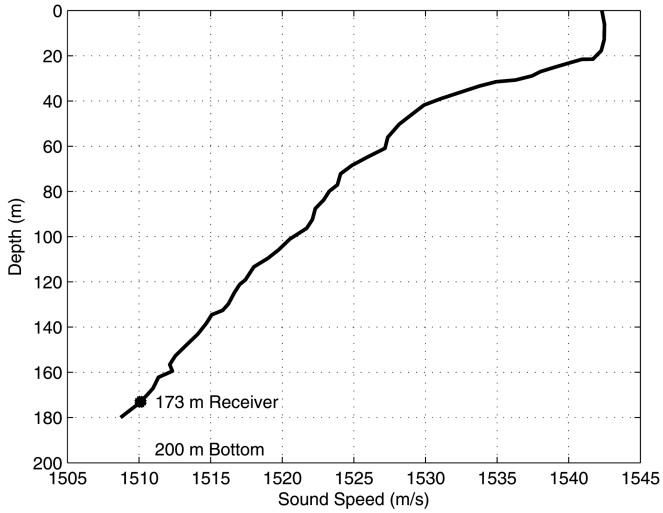

Fig. 3. SSP for GOM environment.

noise from the surface must be combined with other effects, such as flow noise, which depend on receiver characteristics and speed.

This paper describes two sets of midfrequency measurements of vertical noise directionality and characterizes the nature of the observed distributions. The basic physical acoustic mechanisms determining noise directionality are reviewed and the implications for sonar system design are considered. A vertical noise model (VNoise) is described and shown to reproduce the shape of the measured data sets in the downward-refracting environments studied.

II. Midfrequency Data Sets

Measurements of the vertical directionality of midfrequency surface noise have been made in a handful of experiments. The two sample distributions included herein enable the general nature of the distribution to be characterized for downward-refracting environments, i.e., situations in which sound speed decreases with depth. This type of environment was chosen in each of the two experiments to obtain measurements of the low-angle shadow zone or "notch" region [9].

A. Data Set 1—Gulf of Mexico, June 1993

The first of the two data sets was obtained in the Gulf of Mexico (GOM) in June 1993 [10] during a sea test sponsored by the Deployable Acoustic Sensor System (DASS) project. The site of the test was about 100 nmi west of Naples, FL, with the receiver moored at 26° 19′ 78″ N, 84° 23′ 08″ W. The measuring array was part of the U.S. Naval Research Laboratory (NRL, Washington, DC) digital acquisition buoy system (NDABS) and was provided by the Stennis Space Center Division of the Naval Research Laboratory (NRL/SSC, Stennis Space Center, MS) [12]. It was a 31-element vertical line array with −28-dB sidelobes and 0.3-m spacing, and thus, a design frequency of 2500 Hz. The array was moored with its center 27 m above the bottom in 200 m of water as shown in Fig. 2. Individual hydrophone receptions were transmitted to an instrumented pressure vessel where they were digitized at a rate of 6348 Hz and recorded for 30 min every 6 h over an 8-d period.

The array data was processed by performing a fast Fourier transform (FFT) on data from each hydrophone with a transform size of 1024 and a Hanning window, resulting in a 3-dB resolution of approximately 9 Hz. The complex data were then beamformed in each FFT bin using Taylor shading with 28-dB sidelobes. Finally, the beamformed data were magnitude-squared and block-averaged over 128 transforms (approximately 20 s).

Sound-speed profiles (SSPs) were computed from sampled conductivity–temperature–depth (CTD) data at the beginning and end of the test and a fathometer survey indicated a slight bottom slope of about 0.1°. Information provided by the Acoustic Assessments Section of NRL/SSC indicated that the bottom was composed of muddy sand and that other sources of ambient noise such as shipping activity and oil drilling were minimal. A plot of the SSP at the beginning of the test is shown in Fig. 3 with the depth of the receiving array center indicated at 173 m.

A plot of beam power as a function of D/E angle (positive angles are up) and frequency, measured during a time when there was no ambient contribution from biologics or shipping is shown in Fig. 4. The low-angle notch is evident between 500 and 2500 Hz where the array beamwidth is narrow enough to resolve it. Also evident in Fig. 4 are striation patterns which are likely due to a resonance effect in the bottom which consisted of a layer of muddy sand over hard rock. Frequencies with wavelengths which would be trapped in the sediment layer did not return to the water column for multiples of some base frequency. A slice through Fig. 4 at 2473 Hz is shown in Fig. 5. This single frequency plot of beam noise versus D/E angle will be used in the model comparison in Section V.

B. Measured Data Set 2 (DS2)—Tongue of the Ocean, Fall 1988

The second data set was taken from an experiment in September/October 1988 in the Tongue of the Ocean (TOTO)

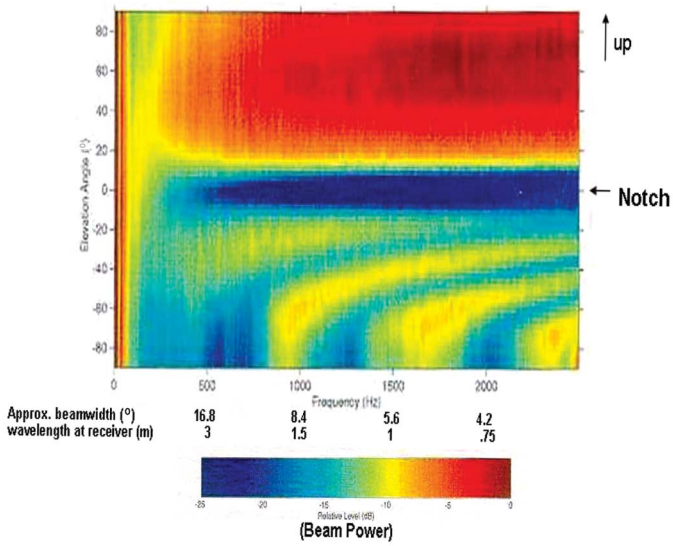

Fig. 4. GOM data as a function of D/E angle and frequency (reproduced from [10]).

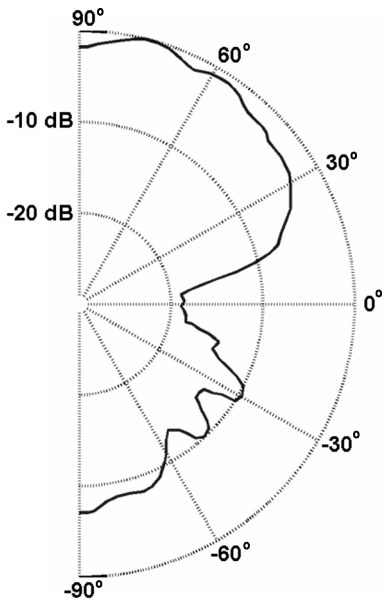

Fig. 5. Slice of GOM data at 2473 Hz (reproduced from [10]).

in the Bahamas at a depth of 200 m in 700 m of water where the bottom depth was variable in the near proximity of the experiment [8].

The measurement system was a deployable acoustic-monitoring system (DAMS) which was specifically designed to measure the vertical distribution of sea surface sound. The wideband system (40 to 4000 Hz) was composed of seven nested arrays of seven hydrophones each, with −18-dB sidelobes. A sketch indicating the hardware components of the system is reproduced from [13] in Fig. 6. The system consists of "seven octavely coalesced four-wavelength acoustic line antennas" [13]. Each antenna section transmitted hydrophone signals to a submerged data logger where they were digitally recorded. A full description of the DAMS system and subsequent processing of the measured noise field is beyond the scope of this paper. An

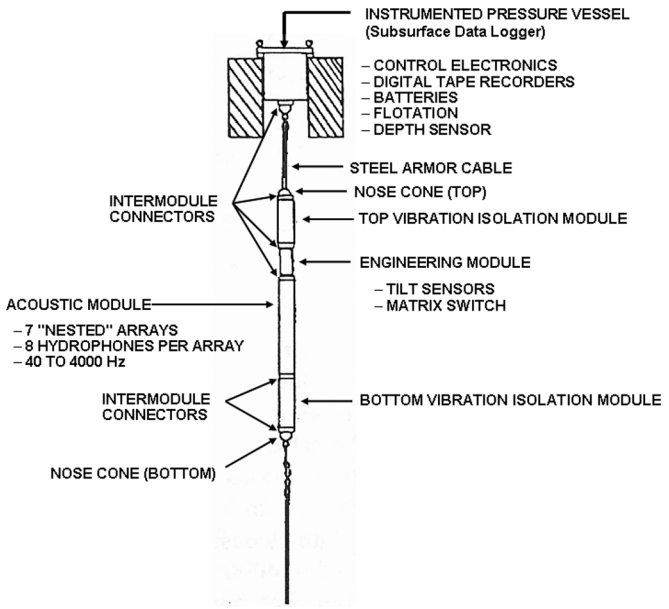

Fig. 6. DAMS system used to collect TOTO data (reproduced from [13]).

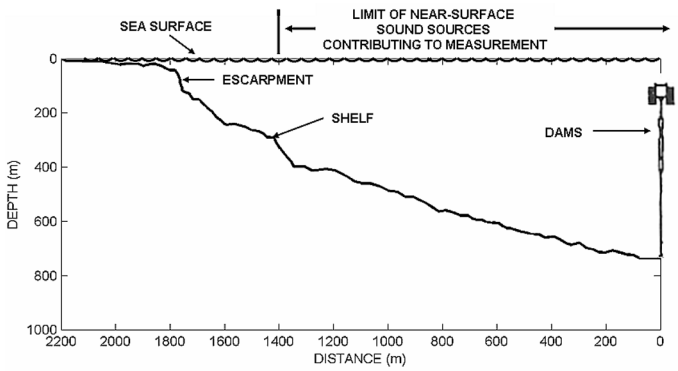

Fig. 7. Illustration of the location of the hydrophone array relative to the ocean surface and ocean bottom for TOTO data (reproduced from [13]).

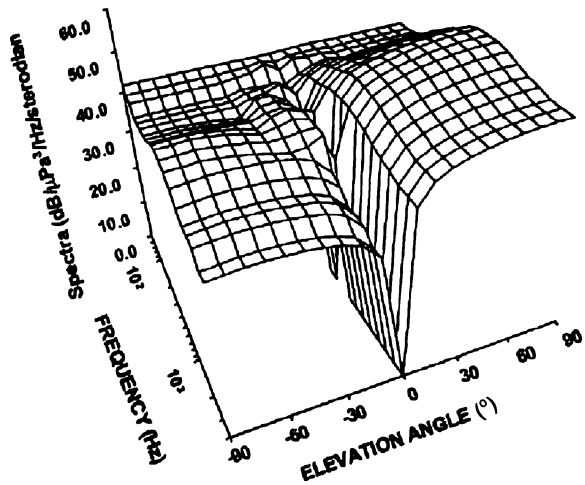

Fig. 8. TOTO vertical noise as a dunction of D/E angle and frequency (reproduced from [15]).

overview can be found in [13] and a detailed system description in [14]. The vertical noise distribution shown in Fig. 8 [15] was

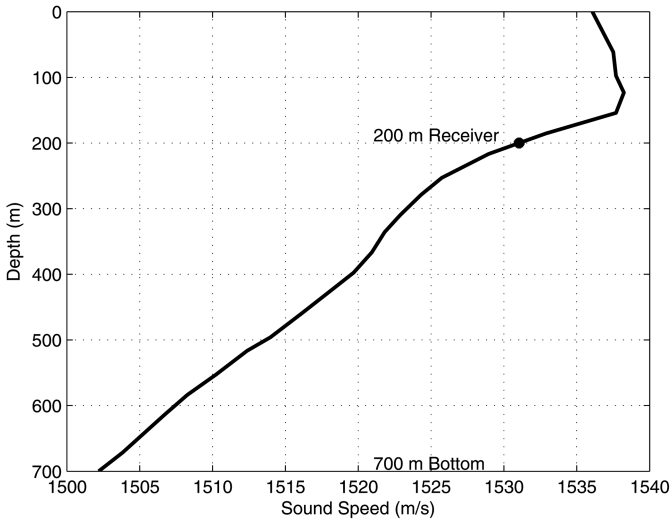

Fig. 9. SSP for TOTO environment.

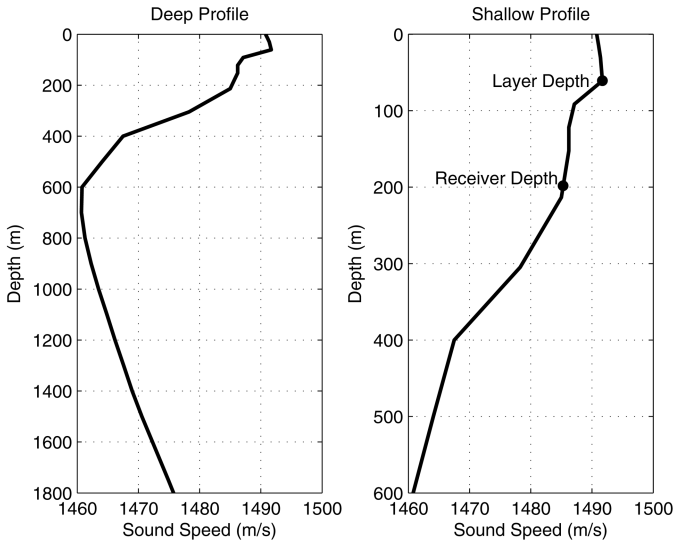

Fig. 10. SSP for Norwegian Sea September sample environment.

derived from the ensemble of cross-spectral density functions for all possible hydrophone pairs (see [15] and [16]). Nuttall [16] has assumed that the inversion method used captured the complete directional spectrum. Thus, the model prediction of the vertical directionality of the 4 kHz noise for the TOTO data set in Section V assumes omnidirectional receive sonar beams.

A plot of the receiver orientation with respect to the sloping bathymetry in the TOTO environment is reproduced from [13] in Fig. 7, and the SSP is shown in Fig. 9 with the depth of the receiving array indicated at 200 m. The measured vertical noise distribution as a function of frequency and vertical angle is shown in Fig. 8. Due to isolation of the TOTO water basin, the ambient noise in the location of the experiment was dominated by local sea surface conditions.

III. Sonar Implications

To illustrate the propagation effects which drive the subsurface vertical directionality of surface noise and to investigate the impact of beam geometry on received beam noise, a location in the Norwegian Sea with a receiver at a depth of 198 m in a water column of 1774 m was used to compute the vertical noise distribution and beam noise for a sample of hypothetical beam patterns. The downward-refracting profile for the sample environment is shown in Fig. 10(a) with an enlarged plot of the shallow profile in Fig. 10(b). The bottom was modeled using high-frequency bottom-loss (HFBL) province 5 and the wind speed was 13 kn, the historical level at this location in the Norwegian Sea for the month of September.

As indicated by the GOM and TOTO data sets discussed in Section II, surface noise at a submerged receiver in downward-refracting environments is vertically nonisotropic, with the highest level at upward-looking beam angles and a lower level at downward-looking beam angles, and is significantly quieter at near-horizontal angles. These three regions correspond, respectively, to noise arriving at the receiver on direct paths from the surface, noise reflected to the receiver from the ocean bottom, and a low-angle notch in which ray paths from the surface arriving at the receiver depth will originate at a great distance from the receiver, and hence, be significantly attenuated. These three regions and their effects on the sample vertical noise curve are depicted in Fig. 11.

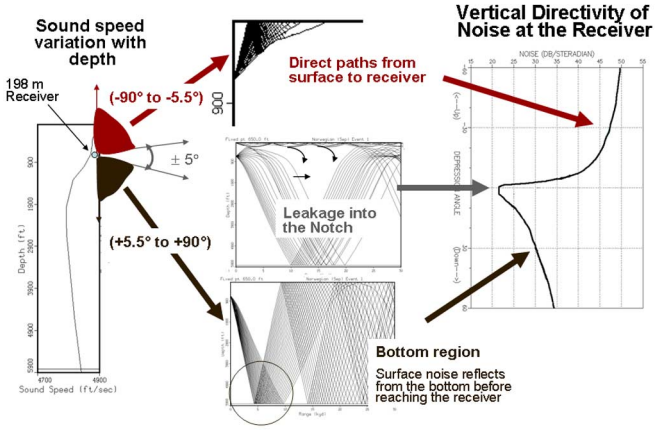

Fig. 11. Ray traces corresponding to angular regions of a sample vertical noise distribution.

The sonar array and beamformer spatially filter the incoming signal and noise fields. The spatial filters or beam patterns are formed at a sufficient number of vertical and azimuthal steer directions to sample all potential signal directions. Both the width of the filter mainlobe and the degree of sidelobe suppression significantly affect the received beam noise level. Fig. 12 depicts beam noise as a function of D/E angle for a set of beams steered at a sample of vertical D/E angles into the environmental vertical noise distribution as shown. The calculation of total beam noise L_N, depicted in Fig. 12, for a single steer angle, involves summing the dot product of the vertical noise level as a function of vertical angle $V(\theta)$ and the vertical beam response as a function of the same vertical angles $B(\theta)$, i.e.,

$$L_N = \int V(\theta) \cdot B(\theta) d\theta.$$

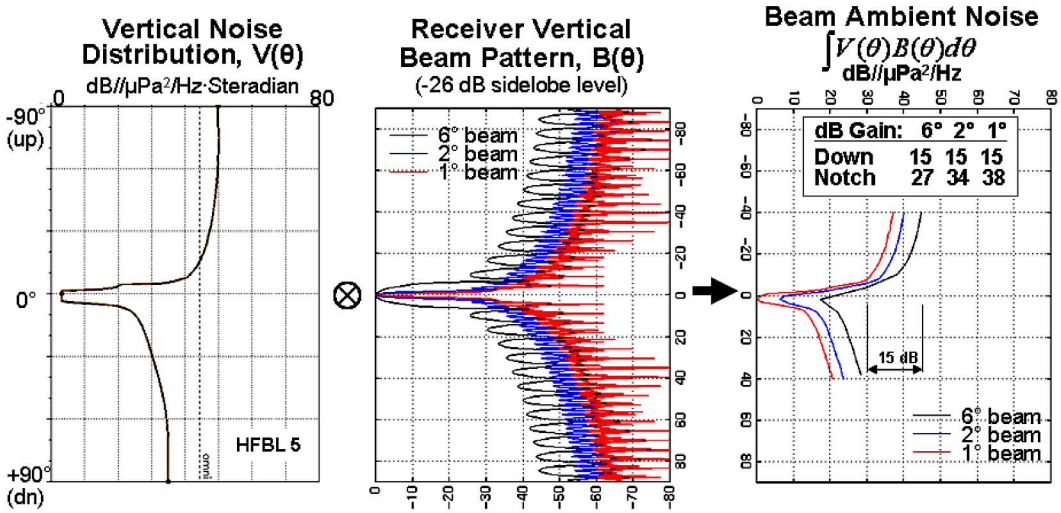

Fig. 12. Beam noise level versus mainlobe beamwidth in sample environment.

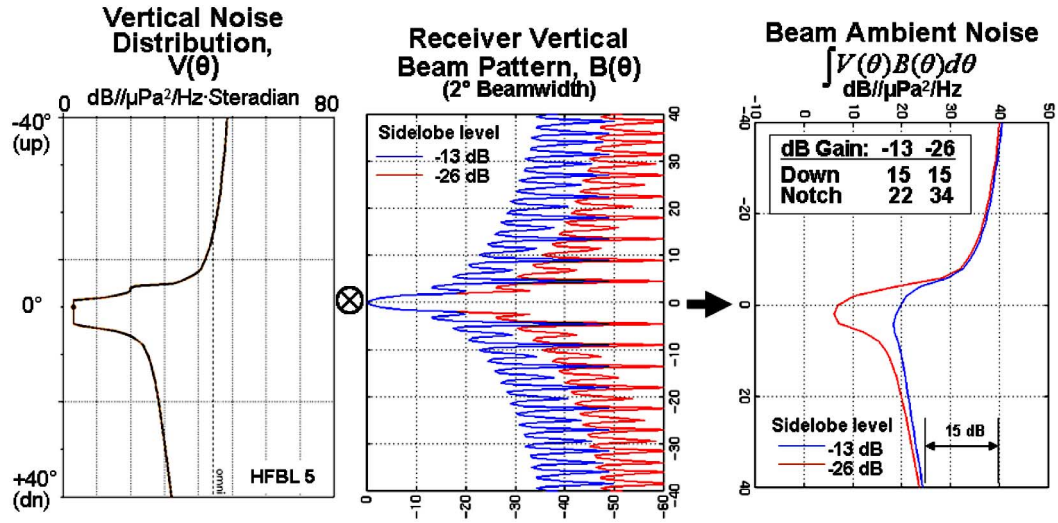

Fig. 13. Beam noise level versus sidelobe level in sample environment.

The vertical axes in the plots in Fig. 12(a) and (b) are vertical direction θ, while the vertical axis in Fig. 12(c) is beam steer angle θ_B. The beam pattern of the 0° D/E angle is shown with 1°, 2°, and 6° beamwidths plotted in red, blue, and black, respectively. The received beam ambient noise levels are plotted for each D/E angle for the 1°, 2°, and 6° mainlobe beamwidths. The suppression of sound in the low-angle notch region increases with the narrowing of the main beam. The comparative noise level between upward- and downward-looking angles of approximately 15 dB, however, is consistent across all three beamwidths. These results suggest the following: 1) a narrow beam relative to the width of the notch improves notch resolution and 2) the difference in gain between downward and upward D/E angles is largely independent of beamwidth.

Since the beam noise level at a given D/E angle represents noise arriving at all vertical angles, sidelobe suppression also significantly impacts the received beam noise level. Fig. 13 shows beam noise as a function of D/E angle for a set of beams against the same hypothetical noise distribution as in Fig. 12, but with sidelobe suppressions of -13 and -26 dB shown in blue and red, respectively, for angles between $\pm 40°$. As in Fig. 12, the vertical axes in Fig. 13(a) and (b) are vertical direction θ, while the vertical axis in Fig. 12(c) is beam steer angle θ_B. The beam noise distributions in Fig. 13(c) differ in that the beam with greater sidelobe suppression shows a lower noise level in the horizontal notch region (over 10 dB of gain) and the gain of 15 dB in downward-looking over upward-looking D/E angles is consistent across beams with both sidelobe levels. These results suggest that increased sidelobe suppression aids in resolution of the low-angle notch.

To further illustrate the effect of sidelobe suppression on beam noise directionality, the noise arriving on the mainlobe of each beam versus that received on sidelobes is shown in Fig. 14 for a beam with mainlobe beamwidth of 2°. At steeper angles in both upward- and downward-looking steer angles, the noise curve is dominated by acoustic energy received in the mainlobe, as the beams in these regions are pointed towards the surface or bottom where the noise levels are highest. For

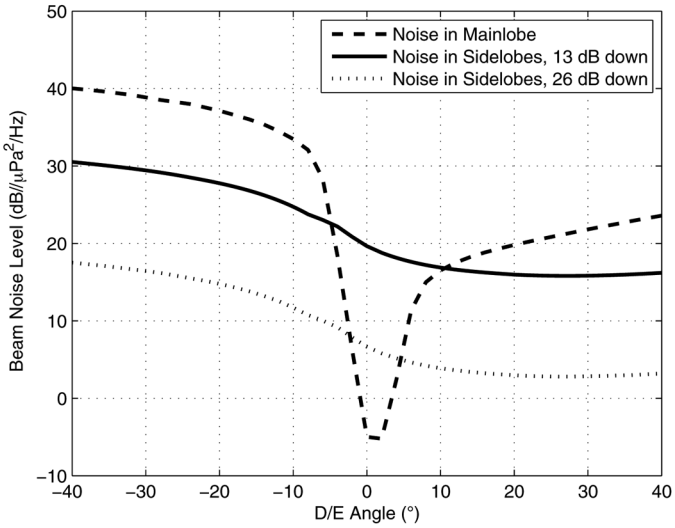

Fig. 14. Beam noise received on mainlobe and sidelobes in sample environment.

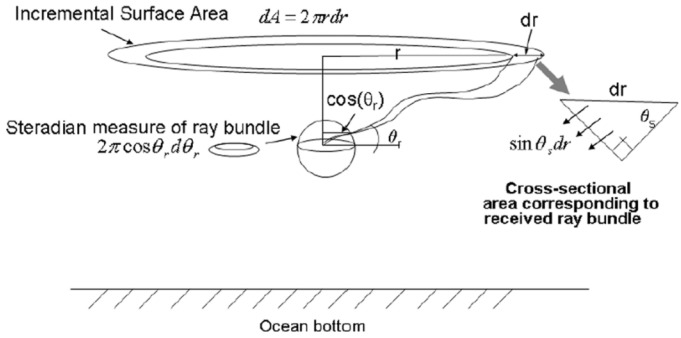

Fig. 15. Overview of modeling approach.

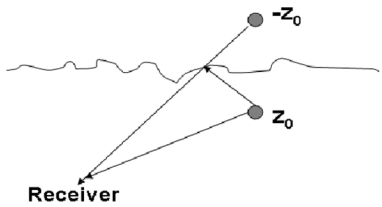

Fig. 16. Source propagation pattern.

beams steered towards the horizontal notch region, the beam noise is dominated by energy impinging on the sidelobes which are directed towards angular regions of higher noise level, i.e., towards the surface and bottom. The change in sidelobe level has no effect on the upward-looking D/E angles where the high level of noise from the surface is received on the mainlobe of the beam, a major impact in the notch where energy is highest in the sidelobes, and a lesser effect on downward-looking D/E angles where the highest level of energy is again received on the mainlobe, but has been attenuated due to bottom reflection.

The previous discussion deals only with the reception of ambient noise by the sonar system beams. In addition, there are other effects, notably flow noise, to be considered. In angular regions where the ambient noise level is low, e.g., in the notch region or at downward-looking angles over an absorbing bottom, the total beam noise may be dominated by flow noise. Furthermore, the tactical relevance of vertical directionality of ambient noise depends on the extent to which it masks a signal of interest. Beam noise gain associated with a narrow mainlobe may be accompanied by loss of signal due to energy splitting, with a resultant decrease in signal-to-noise ratio (SNR). The best SNR may be in a direction that corresponds to neither the strongest signal nor the quietest noise.

IV. Model Description

The noise field at a subsurface receiver due to wind noise at the surface is modeled by integrating the effects of sound propagating to a subsurface receiver from multiple monopole or dipole sources distributed throughout an area of the sea surface. This approach has been used successfully at high frequencies [17]. In this section, we discuss the theoretical development of a vertical noise model based on the integrated mode method of computing propagation documented in [18].

A. Dipole and Monopole Source Factors

In ambient noise modeling, the source of surface noise is generally treated as a field of uniformly distributed subsurface monopoles and/or dipoles distributed throughout an area of the sea surface [8], [17], as depicted in Fig. 15. The model computes an "intensity density" function that represents power per unit of cross-sectional area in units of decibels per micropascal per hertz per steradian. Since steradian measure corresponds to the surface area intersected on a unit sphere with a total surface area of 4π, the conversion from the more familiar omnidirectional decibel level to decibels per steradian is $-10\log_{10}(4\pi)$ or about -11 dB.

For purposes of this paper, we assume a monopole source at depth z_0 below a pressure-release surface and a reflected point source equidistant above the surface as depicted in Fig. 16. The combination of direct and surface- reflected paths results in a dipole-like or "doublet" propagation pattern from the perspective of a subsurface receiver.

Assuming plane-wave propagation, the direct path contribution from the source at z_0 is given by a plane wave

$$e^{-ik_r r}e^{-ik_z(z_r-z_0)}$$

where k_r and k_z are the horizontal and vertical components of the wave number and z_r is the depth of the receiver. The reflected path contribution is another plane wave

$$\mathrm{Re}^{-ik_r r}e^{-ik_z(z_r+z_0)}$$

where R is the complex surface reflection coefficient

$$R = |R|e^{-i\pi}.$$

The total field ψ of the two waves is

$$\psi = e^{-ik_r r}e^{-ik_z(z_r-z_0)} + \mathrm{Re}^{-ik_r r}e^{-ik_z(z_r+z_0)}$$

or

$$\psi = e^{-ik_r r}e^{-ik_z z_r}(e^{ik_z z_0} + \mathrm{Re}^{-ik_z z_0}).$$

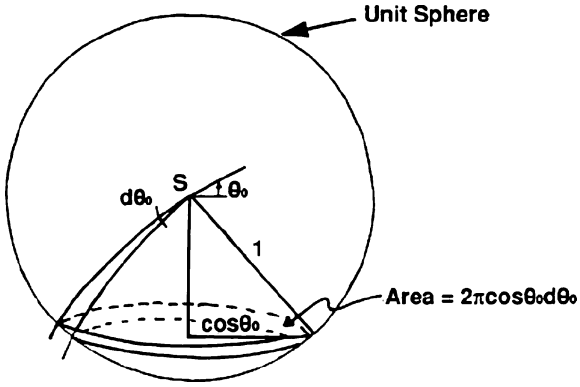

Fig. 17. Steradian coverage of a ray bundle.

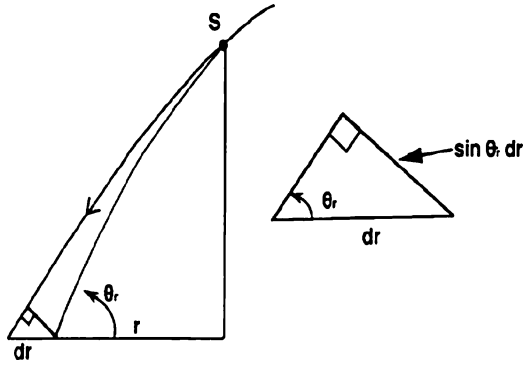

Fig. 18. Cross-sectional area.

The field intensity is $|\psi|^2$ or

$$\psi\psi^* = (e^{ik_z z_0} + \mathrm{Re}^{-ik_z z_0})(e^{-ik_z z_0} + R^* e^{ik_z z_0})$$

where the * denotes complex conjugation, and k_r and k_z are assumed to be real quantities. Simplifying, the field intensity is

$$|\psi|^2 = 1 + |R|^2 - 2|R|\cos(2k_z z_0). \tag{1}$$

If $|R| = 1$, then in terms of angles at the surface, we can write $k_z = k_0 \sin\theta_0$, and the intensity reduces to the dipole pattern

$$|\psi|^2 = 4\sin^2(k_0 z_0 \sin\theta_0). \tag{2}$$

In the noise model, we assume azimuthal invariance and use a source beam B_0 given by

$$B_0(\theta_0) = 1 + |R(\theta_0)|^2 - 2|R(\theta_0)|\cos(2k_0 z_0 \sin\theta_0). \tag{3}$$

For the monopole approximation, the two paths are summed randomly in phase and the intensity is given by

$$B_0(\theta_0) = 1 + |R(\theta_0)|^2. \tag{4}$$

B. Approximate Ray Theoretic Analysis

To illustrate the method in a simplified context, we first derive an expression for the vertical distribution of surface noise at a submerged receiver based on ray theoretic considerations. Under certain conditions (e.g., high-frequency propagation with $\theta_r > 30°$), the ray theoretical expression is valid, but for small θ_r (e.g., convergence zone propagation with $\theta_r \leq 15°$), and especially at low frequencies, a propagation model such as the integrated mode method which is capable of computing diffraction is required.

Consider the intensity of a ray bundle of width $d\theta_0$ emitted from a point at the surface at an angle of θ_0 and arriving at a subsurface receiver at an angle of θ_r as depicted in Figs. 17 and 18. The intensity along the ray bundle at a given horizontal range is related to the number of steradians per unit of cross-sectional area at that range, where the steradian measure of the ray bundle is equal to the surface area intersected on a unit sphere. The area is intersected approximated by $A_0 = 2\pi\cos\theta_0 d\theta_0$ as illustrated in Fig. 17.

To compute the cross-sectional area that is covered by the same ray bundle at range r, consider the geometry of Fig. 18. The cross-sectional area is $A_r = 2\pi r \sin\theta_r dr$. The amount of ray bundle spreading as compared to that on the unit sphere is given by the ratio A_r/A_0. The sound intensity, which expresses the amount of spreading of the ray bundle after reaching range r, is proportional to the reciprocal of the area ratio. Thus

$$\frac{I}{I_0} = \frac{A_0}{A_r}.$$

By taking the reference intensity I_0 to be unity, then

$$I = \frac{\cos\theta_0}{r\sin\theta_r\left(\dfrac{dr}{d\theta_0}\right)}.$$

Since we express angle relationships in terms of θ_r, we use Snell's Law to replace $\cos\theta_0$ by

$$\frac{c_0}{c_r}\cos\theta_r$$

where c_0 and c_r are the sound speed at the surface and receiver depth, respectively. Thus

$$I = \frac{c_0}{c_r}\frac{1}{r\dfrac{dr}{d\theta_0}}\frac{\cos\theta_r}{\sin\theta_r}. \tag{5}$$

Now consider an annular region on the surface with radius r and width dr as shown in Fig. 15.

Assuming, for the moment, a density of noise sources with unit strength per unit of area, the contribution of the differential area dA at the receiver is IdA, which is given by substituting $dA = 2\pi r dr$ into (5) as

$$IdA = \left[2\pi\frac{c_0}{c_r}\frac{\cos\theta_r}{\sin\theta_r}\right]d\theta_0.$$

Thus, the quantity in brackets represents an "intensity density" function in terms of θ_0. This expression can be extended to include azimuthal variation by recognizing that the 2π factor results from integration over azimuthal angle ϕ, i.e.,

$$\int_0^{2\pi} d\phi = 2\pi.$$

TABLE I
MULTIPATH/ANGLE CORRESPONDENCE

Path	Source Angle	Receive Angle
(1)	down	up
(2)	up	up
(3)	down	down
(4)	up	down

Thus, the "intensity density" V in both horizontal (θ) and vertical (ϕ) directions is given by

$$V(\theta_0,\phi)d\theta_0 d\phi = \frac{c_0}{c_r}\frac{\cos\theta_r}{\sin\theta_r}d\theta_0 d\phi.$$

Since we wish to express the vertical angle density in terms of the receive vertical angle θ_r, we perform the change of variable

$$\theta_0 = \cos^{-1}\left[\frac{c_0}{c_r}\cos\theta_r\right]$$

to obtain density in θ_r as

$$V(\theta_r,\phi)d\theta_r d\phi = \left(\frac{c_0}{c_r}\right)^2 \frac{\cos\theta_r}{\left(1-\sqrt{\left(\frac{c_0}{c_r}\right)^2\cos^2\theta_r}\right)}d\theta_r d\phi. \tag{6}$$

This result corresponds to the model presented in [19] and [20].

C. Integrated Mode Formulation of Vertical Noise Distribution

The discussion in Section IV-B describes the sequence of calculations used to construct the surface noise field at the receiver using simple ray theory. In the VNoise model described herein, the same development applies except that the propagation of energy from each source to the receiver is computed by the integrated mode method described in [18]. In particular, consider an integral corresponding to path l where $l = 1, 4$ as summarized in Table I and ray path cycle q where $q = 0, 1, \ldots$

$$I_{lq} = \frac{1}{\sqrt{2\pi r}}\int_{k_1}^{k_2}\sqrt{k_r A(z_r,k_r)A(z_0,k_r)} \times e^{-i(k_r r + h_\Gamma(k_r))}dk_r \tag{7}$$

where r is a horizontal range, k_r is a horizontal wave number, k_1 and k_2 identify upper and lower turning points or boundary reflections, $h_\Gamma(k_r)$ is an elapsed vertical phase along path Γ, $A(z_r,k_r)$ and $A(z_0,k_r)$ are wave amplitudes at receiver and source, respectively, and a ray path cycle is defined as propagation from one upper turning point or reflection to the next. For convenience, we omit boundary losses for the moment so the treatment parallels that of Section IV-B.

As in [18], the notation for path type is such that $l = 1, 2$ represent propagation paths arriving at the receiver from above and $l = 3, 4$ represent propagation paths arriving from below. Cycle $q = 0$ represents the direct path, which proceeds from a given surface source at depth z_0 to the receiver at depth z_r. In the case depicted in Fig. 16, the combined path arrives at the receiver from the upward direction and thus paths $l = 1, 2$ correspond to the two paths in Fig. 16. With a suitable boundary condition accounted for, the coherent combination of these two paths produces the acoustic field of a dipole-like or doublet source at the receive point as discussed in Section IV-A.

In the VNoise model, the source function $B_0(\theta_0)$ is included in the integrations (7) and paths $l = 2, 4$ are omitted. With surface and bottom reflection coefficients R_1 and R_2, respectively, the general integral form (7) with $\sqrt{k_r A(z_r,k_r)A(z_0,k_r)}$ replaced by A becomes

$$I_{lq} = \frac{1}{\sqrt{2\pi r}}\int_{k_1}^{k_2} B_0(\theta)AR_1^p(R_1R_2)^q \times e^{-i(k_r r + h_{\Gamma,lq}(k_r))}dk_r \tag{8}$$

where $p = 0$ for $l = 1$ and $p = -1$ for $l = 3$, and $h_{\Gamma,lq}$ indicates vertical phase along path Γ for path type l and cycle q.

The derivation of an expression for the vertical distribution of surface noise at the receiver proceeds in parallel with the development in Section IV-B, i.e., the integrals in (8) are converted to sound intensity and the contributions of individual sources are integrated over surface area.

D. Calculation of Beam Noise and Noise Gain

Noise gain, or the improvement in SNR due to reduction in ambient noise due to the directional discrimination of a given sonar beam, is given by [21] as a function of solid angle Ω as

$$N_{\mathrm{AG}} = 10\log_{10}\frac{\int N(\Omega)B(\Omega)d\Omega}{\int N(\Omega)d\Omega} \tag{9}$$

where $B(\Omega)$ is the receive beam pattern. In the VNoise model, the noise distribution is normalized so that integration over solid angle Ω yields the midfrequency omnidirectional ambient noise level as a function of wind speed or sea state and frequency according to the Wenz curves [1]. As a function of horizontal and vertical angles ϕ and θ, the total omnidirectional noise level is given by

$$L_N = \int\int V(\theta)\cos(\theta)d\theta d\phi = \int V(\Omega)d\Omega. \tag{10}$$

Beam ambient noise LE_B for a given frequency and environment is computed by convolving the noise $V(\theta,\phi)$ with the beam pattern $B(\theta,\phi)$ at each steer D/E angle θ_B and integrating the result over azimuth ϕ, i.e.,

$$\mathrm{LE}_B(\theta_B) = \int\int V(\theta,\phi)\cdot B(\theta,\phi)\cos(\theta)d\theta d\phi. \tag{11}$$

Finally, total beam noise $\mathrm{LE}_{B\mathrm{tot}}$ is the power sum of the ambient noise with the flow noise L_e for a given receive platform and speed. The SNR for a given target is computed by comparing the noise $\mathrm{LE}(\theta_B)$ to the received signal level on a beam-by-beam basis.

V. COMPARISON OF MODEL RESULTS TO MEASURED DATA SETS

Plots comparing the modeled and measured vertical noise distributions for the GOM and TOTO environments of Section II are shown in Figs. 19 and 20, respectively. In both plots, the measured values are shown as solid dots and the model prediction is represented by a solid line.

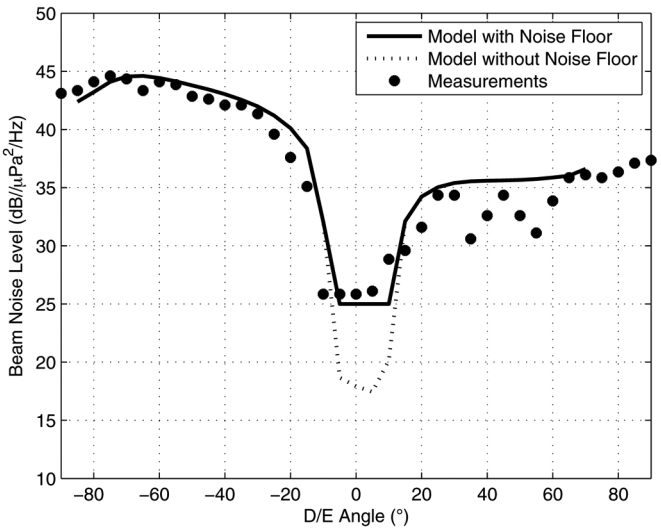

Fig. 19. Modeled versus measured noise for the GOM environment (2473-Hz DASS data).

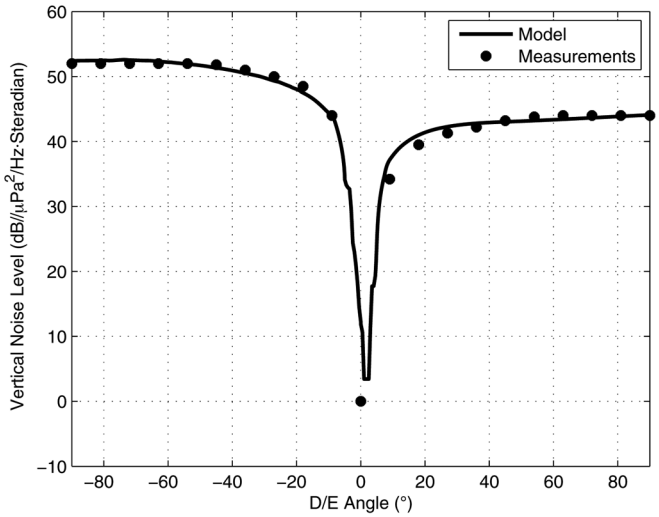

Fig. 20. Modeled versus measured beam noise for the TOTO environment.

A sea state level of 2 was assumed for the GOM data set, an estimate obtained from [10], and the modeled beam pattern is shown in Fig. 21. The bottom was modeled as province 2 according to the HFBL data base from the Oceanographic and Atmospheric Master Library [22], which is valid for frequencies between 1.5 and 4.0 kHz, because it most closely matches the bottom loss predicted by modified acoustic bottom loss evaluation (ABLE) [11] province 1 used in [10]. An unidentified noise source resulted in a notch floor in the measurements of about 25 dB which is not predicted by the model.

For the TOTO data set, a wind speed of 25 kn and HFBL province 2 were used. Since the model normalizes the vertical noise distribution to match the overall omnilevel predicted for a given sea state and frequency according to the Wenz curves [1], a wind speed of 25 kn and a bottom type of HFBL province 2 resulted in a match to the level of the measured data. Although there is no basis for these assumptions other than matching to the data, the shape of the noise distribution has been successfully reproduced by the model. The modeled distribution is $V(\theta)$

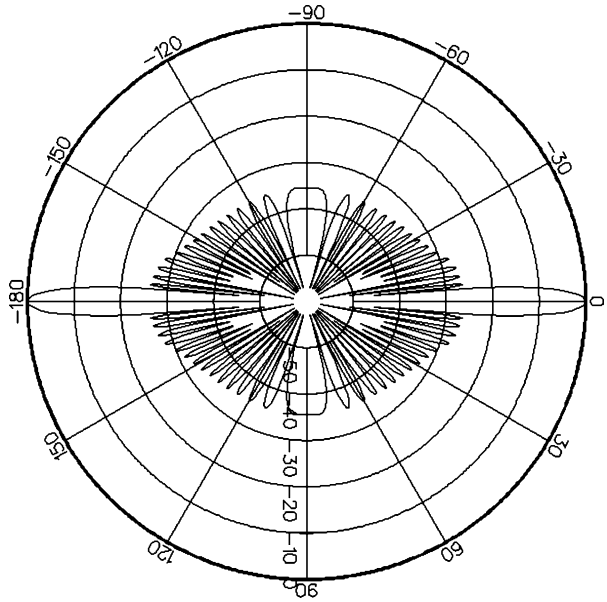

Fig. 21. NDABS beam pattern at steer angle 0° (horizontal).

rather than $\mathrm{LE}(\theta_B)$ because no beam was applied. The inversion method used in processing the data is believed to have recovered the full directional spectrum of the measured noise field [16], as discussed in Section II.

The source model $B_0(\theta)$ is the effective dipole (3) of Section IV-A, which represents the interference pattern between a monopole located below the pressure-release surface and its image above the surface. To control phase interference patterns as frequency is increased, the product of horizontal wave number k times source depth z_s, which appears in (3) for the dipole, has been set equal to a constant value of 1/3, a constant previously chosen by comparison with measured data. To test the effectiveness of this assumption with respect to the current data sets, the predictions for the GOM and TOTO environments were repeated using a number of possible source functions. The six functions modeled are as follows:

1) function proposed by Becken [23] given by

$$B_0(\theta_0) = \sin^x \theta_0$$

where

$$x = \begin{cases} 2, & \theta_0 < 20^\circ \\ \frac{\theta_0}{10}, & \theta_0 \geq 20^\circ \end{cases}; \tag{12}$$

2) dipole pattern suggested by Carey [24] given by

$$B_0(\theta_0) = 1 + |R(\theta_0)|^2 - 2|R(\theta_0)| \cos(2kz_s \sin\theta_0)$$

where k is a horizontal wave number and the source depth z_s is set equal to $\lambda/4$ where λ is a wavelength, i.e., the product of kz_s is always equal to $\pi/2$;
3) $\sin(\theta_0)$;
4) $\sin^2(\theta_0)$;
5) dipole used herein, i.e.,

$$B_0(\theta_0) = 1 + |R(\theta_0)|^2 - 2|R(\theta_0)| \cos(2kz_s \sin\theta_0)$$

where $z_s = 1$ yard and $kz_s = 1/3$;
6) monopole source function $1 + |R(\theta_0)|^2$.

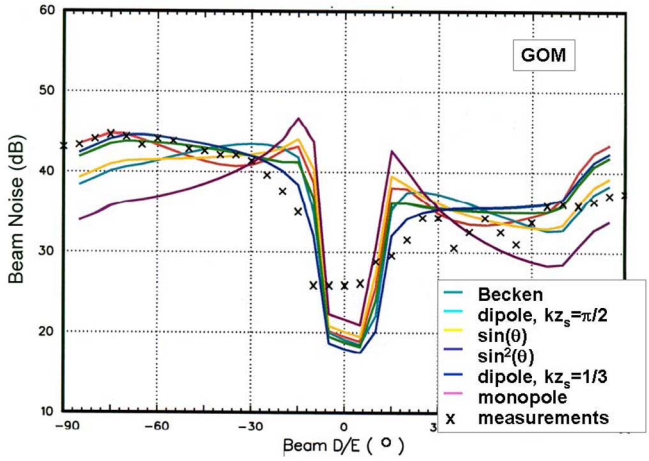

Fig. 22. Comparison of GOM measurements with modeled vertical noise for various source functions.

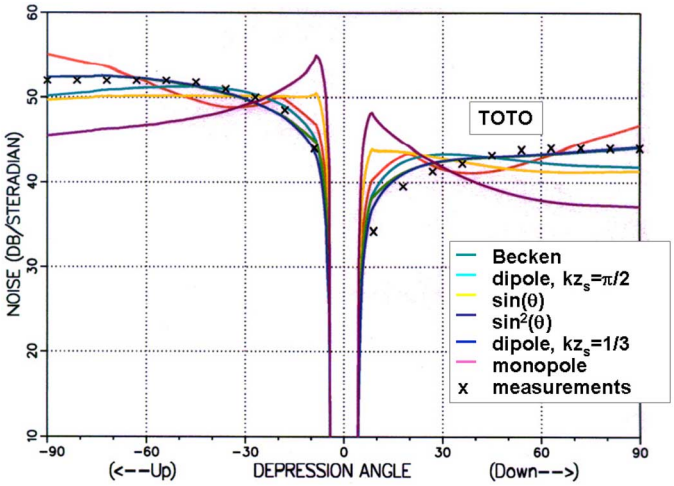

Fig. 23. Comparison of TOTO measurements with modeled vertical noise for various source functions.

Although the source function used currently has no theoretical basis to defend it, the results of the comparison shown in Figs. 22 and 23 for GOM and TOTO, respectively, indicate that the best agreement with the two data sets studied is achieved by its use. Further research is needed to derive a more rigorous source function.

VI. Summary

In summary, it is noted that the undersea environment can provide a strong vertical noise directionality, especially when the SSP is downward refracting. The highest noise arrives at a subsurface receiver from upward directions. A significant quiet region exists at near-horizontal directions in downward-refracting environments and the noise from downward-looking directions is attenuated according to the nature of the bottom. The major features of the vertical noise distribution have been discussed in terms of the physical mechanisms which cause the directionality. The impact on beam geometry for a subsurface receiver with respect to noise suppression and signal detection have been investigated. The VNoise model successfully reproduces the shape of the measured midfrequency vertical noise distributions studied.

Acknowledgment

The author would like to thank R. C. Manke (Code HQ10A) and F. J. Pope (Code 15E1) of the Naval Undersea Warfare Center Division Newport, RI, and W. M. Carey and J. R. Short (formerly of NUWC Division Newport) for their insightful contributions and support of this work. Portions of this paper are also included in Technical Documents of the Naval Undersea Warfare Center [25], [26].

References

[1] G. M. Wenz, "Acoustic ambient noise in the ocean: Spectra and sources," *J. Acoust. Soc. Amer.*, vol. 34, pp. 1936–1956, 1962.

[2] W. A. VonWinkle and D. G. Browning, "Vertical noise directionality in the deep ocean: A review," Naval Underwater Systems Center, New London, CT, NUSC Tech. Document 7561, Dec. 1985.

[3] R. J. Urick, *Ambient Noise in the Sea*. Los Altos, CA: Peninsula, 1984.

[4] W. M. Carey, J. W. Fitzgerald, and D. G. Browning, "Low frequency noise from breaking waves," Naval Underwater Systems Center, New London, CT, NUSC Tech. Document 8783, July 1990.

[5] B. R. Kerman, Ed., *Sea Surface Sound, Natural Mechanisms of Surface Generated Noise in the Ocean*. Norwell, MA: Kluwer, 1988.

[6] B. R. Kerman, Ed., *Natural Physical Sources of Underwater Sound*. Norwell, MA: Kluwer, 1993.

[7] M. J. Buckingham and J. R. Potter, *Sea Surface Sound'94*. Singapore: World Scientific, 1995.

[8] R. M. Kennedy, T. K. Szlyk, and S. M. Wentworth, "Wind speed dependence of acoustic ambient vertical directional spectra at high frequency," Naval Underwater Systems Center, West Palm Beach, FL, NUSC Tech. Rep. 8537, 1989.

[9] V. C. Anderson, "Variation of the vertical directionality of noise with depth in the North Pacific," *J. Acoust. Soc. Amer.*, vol. 66, no. 5, pp. 1446–1452, Nov. 1979.

[10] D. Wilson and R. Kneipfer, Preliminary results of experiment to measure vertical directionality of ambient noise in shallow water Naval Undersea Warfare Center (NUWC), Newport, RI, Tech. Rep., 1995, unpublished.

[11] T. G. Bell, "Wideband ABLE: A total energy bottom loss model for frequencies from 50 to 3500 Hertz," Sonalysts Rep. BLO-0501-003, Oct. 1990.

[12] C. Orr, M. Thiele, W. Johnson, and D. Small, "NRL acoustic array systems," *Sea Technol.*, vol. 34, no. 3, pp. 37–42, Mar. 1993.

[13] R. M. Kennedy and T. V. Goodnow, "Measuring the vertical directional spectra caused by sea surface sound," *IEEE J. Ocean. Eng.*, vol. 15, no. 4, pp. 299–310, Oct. 1990.

[14] R. M. Kennedy and T. V. Goodnow, "Ambient vertical directional spectra at a TOTO near-reef site," Naval Underwater Systems Center, Newport, RI, NUSC Tech. Rep. 8579, Aug. 1989.

[15] R. M. Kennedy, "Measuring the vertical directional spectra caused by sea surface sound," Naval Underwater Systems Center, West Palm Beach, FL, NUSC Tech. Document 8733, 1990.

[16] A. H. Nuttall, "Estimation of noise directionality spectrum," Naval Underwater Systems Center, New London, CT, NUSC Tech.l Rep. 4345, Sep. 1972.

[17] R. M. Kennedy, "Statistical properties of the sea surface sound dipole source," Naval Underwater Systems Center, New London, CT, NUSC Tech. Document 8803, Dec. 1990.

[18] C. A. Clark, "Acoustic wave propagation in horizontally variable media," *IEEE J. Ocean. Eng.*, vol. 30, no. 1, pp. 188–197, Jan. 2005.

[19] G. R. Fox, "Ambient-noise directivity measurements," *J. Acoust. Soc. Amer.*, vol. 36, no. 8, pp. 1537–1540, Aug. 1964.

[20] R. J. Talham, "Ambient-sea-noise model," *J. Acoust. Soc. Amer.*, vol. 36, pp. 1541–1544, 1964.

[21] W. S. Burdic, *Underwater Acoustic System Analysis*. Englewood Cliffs, NJ: Prentice-Hall, 1991, ch. 10.

[22] *Oceanographic and Atmospheric Master Library Summary*, , Oct. 2002, Naval Oceanographic Office, Systems Integration Division, Stennis Space Center, MS.
[23] B. A. Becken, "The directional distribution of ambient noise in the ocean," Mar. Phys. Lab., Scripps Inst. Oceanogr., La Jolla, CA, MPL Scripps 35283, Mar. 1961.
[24] W. M. Carey, "Near surface ambient noise sources," Naval Undersea Warfare Cntr., Newport, RI, NUWC Code 20, Jul. 2001.
[25] D. F. Yarger, C. A. Clark, and G. A. Leibiger, "Low frequency vertical noise model," Naval Underwater Syst. Cntr., New London, CT, NUSC Tech. Rep. 8975, Oct. 1991.
[26] C. A. Clark and F. J. Pope, "Vertical directionality of mid-frequency surface noise," Naval Underwater Syst. Cntr., Newport, RI, NUWC Tech. Memo 04-042A, Sep. 2004.

Cathy Ann Clark (S'03–M'04) received the B.S. degree in mathematics from Morehead State University, Morehead, KY, in 1970, the M.S. degree in mathematics from the University of Connecticut, Storrs, in 1976, and the M.S. degree in electrical engineering and the Ph.D. degree in applied mathematics with an emphasis on nonlinear rational difference equations from the University of Rhode Island, Kingston, in 2001 and 2004, respectively.

She was a Communications Systems Analyst at Western Union Corporation, Mahwah, NJ, from 1969 to 1973. From 1973 to 1979, she was a Lecturer in mathematics at the University of Connecticut and various community colleges in Connecticut. From 1979 to 1997, she was with Sonalysts, Inc., Waterford, CT, working on underwater sound propagation modeling, satellite communications, and submarine tactical decision aid development. Since 1997, she has been with the Sensors & Sonar Systems Department, Naval Undersea Warfare Center, Newport, RI. Her research interests include underwater acoustics, boundary value problems, and difference equations.

Dr. Clark is a member of the American Mathematical Society, the Society for Industrial and Applied Mathematics, and the International Society of Difference Equations.